The fully kinetic Biermann battery and associated generation of pressure anisotropy

K. M. Schoeffler,[1] N. F. Loureiro,[2] and L. O. Silva[1]

[1] *GoLP/Instituto de Plasmas e Fusão Nuclear, Instituto Superior Técnico, Universidade de Lisboa, 1049-001 Lisboa, Portugal*

[2] *Plasma Science and Fusion Center, Massachusetts Institute of Technology, Cambridge MA 02139, USA*

(Dated: March 1, 2018)

The dynamical evolution of a fully kinetic, collisionless system with imposed background density and temperature gradients is investigated analytically. The temperature gradient leads to the generation of temperature anisotropy, with the temperature along the gradient becoming larger than that in the direction perpendicular to it. This causes the system to become unstable to pressure anisotropy driven instabilities, dominantly to electron Weibel. When both density and temperature gradients are present and non-parallel to each other, we obtain a Biermann-like linear in time magnetic field growth. Accompanying particle in cell numerical simulations are shown to confirm our analytical results.

Introduction. Both the seed field required for the generation of astrophysical magnetic fields [1, 2] and intense magnetic fields generated in laser-solid interaction laboratory experiments [3–6] have been attributed to the Biermann battery [7]. The Biermann battery mechanism generates magnetic fields due to non-parallel temperature and density gradients. Until now, the understanding of this mechanism has been restricted to fluid models where an extra non-ideal term is added to Ohm's law. In weakly or non-magnetized plasmas, the validity of fluid models rests on collisions being sufficiently frequent compared to the dynamic timescales of the problem, such that the pressure tensor remains in scalar form [8]. These conditions are often not present in astrophysical environments and are questionable in some laser-plasma environments, and thus a fully kinetic model is necessary.

Recently, the Biermann battery has been investigated with fully self-consistent kinetic 3D simulations [9, 10], but a clear theoretical model for how the fully kinetic Biermann battery actually works in collisionless plasmas has not been fully presented. Such a model is presented here explaining not only the kinetic Biermann battery, but also, more generally, the dynamical evolution of collisionless unmagnetized plasmas subject to background density and temperature gradients. In addition to extending the validity of the Biermann battery to many weakly collisional scenarios, we reveal the purely kinetic result that a temperature gradient alone leads to the generation of anisotropies in temperature (pressure tensor). Ref. [11] further generalizes this model showing both the generation of magnetic fields by the Biermann battery, and the development of temperature anisotropies for arbitrary temperature and density gradients. However, in this Letter we fully frame and justify the assumptions that underlie the model's validity and show how the analytic expression for the time evolution of the momentum distrubution can be applied to address pertinent physical questions. Particularly, unique to this paper, we present discussion of the onset of kinetic instabilities, driven by the temperature anisotropy, such as the Weibel instability [12], seen in [9, 10], or instabilities that inhibit the heat flux [13, 14] on time scales short compared to the collision time. This is relevant for a wide variety of settings including astrophysical shocks and laser experiments with small collision rates, and addresses the low heat flux of cooling flows in galaxy clusters, which cannot be explained by collisional fluid models [15].

Model. We solve the time evolution of the velocity distribution function and electromagnetic fields according to the coupled Vlasov and Maxwell's equations, assuming that only the electrons play a role and the ions are static, only acting as a neutralizing background. For our calculation, we normalize the velocity $\boldsymbol{v}$ to $v_{T0} \equiv \sqrt{T_e/m_e}$, time t to ω_{pe}^{-1}, and $\boldsymbol{x}$ to λ_D, where ω_{pe} is the plasma frequency for density $n = n_0$, and $\lambda_D \equiv v_{T0}/\omega_{pe}$ is the Debye length. In addition E and B are normalized to $E_0 \equiv m_e v_{T0}\omega_{pe}/e$ and $B_0 \equiv m_e c\omega_{pe}/e$ respectively.

We will assume that a background Maxwellian distribution function, f_M, is instantaneously perturbed such that

$$n = n_0\left(1+\epsilon x\right),\; v_T = v_{T0}\sqrt{1+\delta y}, \tag{1}$$

$$\epsilon \equiv \frac{\lambda_D}{L_n} \equiv \lambda_D \frac{1}{n}\frac{\partial n}{\partial x}\left(0\right),\; \delta \equiv \frac{\lambda_D}{L_T} \equiv \lambda_D \frac{1}{T}\frac{\partial T}{\partial y}\left(0\right). \tag{2}$$

This perturbation is not an equilibrium solution; it will be taken as a given initial state. The Biermann battery is simply the time evolution of the initial non-equilibrium state, not an instability (note that in fluid models it grows linearly, not exponentially, with time; we will find here that this remains true in the kinetic case). The initial non-equilibrium state, which can be generated by violent interactions with lasers or shocks, is itself the source of free energy which generates the magnetic field. The finite spot-size of laser interactions, or the finite extent of shock fronts will rapidly give rise to a temperature gradient perpendicular to the density gradient, which is necessary for the Biermann battery. Furthermore, we will explain in the conclusion how our solution can be applied

to an anisotropic temperature distribution, which is expected in such experimental setups. However, one should note that in this simplified model of our initial state, we ignore for example magnetic fields induced by the initial laser interaction, and heat flux or temperatures that are initially evolving with time.

The parameters ϵ and δ are taken to be very small and comparable to each other; they will be used as our asymptotic expansion coefficients. Assuming $\boldsymbol{x} \sim \epsilon^0$, the initial distribution function to second order in ϵ and δ is:

$$f_0 = f_M + \epsilon x f_M - \frac{1}{2}\delta y \left(3 - v^2\right) f_M + \frac{1}{8}\delta^2 y^2 \left(15 - 10v^2 + v^4\right) f_M - \frac{1}{2}\epsilon\delta x y \left(3 - v^2\right) f_M. \tag{3}$$

We evolve the Vlasov-Maxwell equations initialized with this distribution function, and either no initial electric or magnetic fields, or equilibrium fields that act to balance the force due to the pressure gradient.

The evolution of the electron distribution function subject to these density and temperature gradients is given by the Vlasov equation, coupled with Faraday's and Ampere's laws:

$$\frac{\partial f}{\partial t} + \mathbf{v}\cdot\boldsymbol{\nabla} f - (\mathbf{E} + \mathbf{v}\times\mathbf{B})\cdot\boldsymbol{\nabla}_v f = 0, \tag{4}$$

$$\frac{\partial \mathbf{B}}{\partial t} = -\boldsymbol{\nabla}\times\mathbf{E}, \tag{5}$$

$$\frac{\partial \mathbf{E}}{\partial t} = \int d^3v \mathbf{v} f + \frac{c^2}{v_{T0}^2}\boldsymbol{\nabla}\times\mathbf{B}. \tag{6}$$

We will seek solutions to these equations in powers of ϵ and δ. We will assume $t \sim \boldsymbol{x} \sim c^2/v_{T0}^2 \sim \epsilon^0 \sim \delta^0$. Although the solution is only valid when $\boldsymbol{x} \sim \epsilon^0$, at an arbitrary position $\boldsymbol{x}$, the calculation remains valid in a new coordinate system $\boldsymbol{x}'$, where the assumptions are satisfied using ϵ' calculated with the local v'_{T0} and n'_0. There are three other small parameters besides ϵ and δ; namely c_s/v_{T0}, v_{T0}^2/c^2, and ν/ω_{pe}, where c_s is the sound speed, and ν is the collision frequency. Each of these parameters are assumed to be much smaller than one, but aside from ν/ω_{pe}, can in principle (and must in the case of v_{T0}^2/c^2 [16]) remain of order ϵ^0. We implicitly assume small values for these parameters by assuming static ions, using the non-relativistic Vlasov equation/ Maxwellian distribution, and ignoring collisions.

First we highlight some important aspects of the form of the solution. The first order ($\sim \epsilon^1$) solution including all terms proportional to c_s/v_{T0} and v_{T0}^2/c^2, of $\boldsymbol{E}$, and f is uniform in space, and f is an odd function of v. A proof of this is provided in the supplementary materials. Given a uniform E, from Eq. (5) no magnetic field is generated, and an odd f with respect to v only leads to uniform bulk flows and temperature fluxes. It is thus necessary that we perform our calculation with second order terms ($\sim \epsilon^2$) to see the Biermann battery, and the formation of a temperature anisotropy. The second order solution is different in form, and except for terms of f which are even in v, there are no terms that are uniform in space. It should be emphasized that this means that modifications coming from c_s/v_{T0} and v_{T0}^2/c^2 can be separately neglected for both first order and second order solutions. Note that second order modifications to the first order solution are then neglected (the entire solution is not accurate to ϵ^2).

Solutions can be found from an initial condition by taking an expansion for small t, restricted to second order in ϵ. Fortunately, the sum over all orders of t converges to a solution valid for arbitrary $t \sim \epsilon^0$, and thus only small compared to the electron transit time $L_T/v_{T0} = \delta^{-1}$.

Density gradient. We first consider the case with only a density gradient ($\delta = 0$). If we assume the initial condition of $f = f_0$ and no initial electric or magnetic fields, we obtain the following analytic solution:

$$f = f_0 + \tilde{f}_n(t), \tag{7}$$

$$\boldsymbol{E} = -\left(\epsilon - \epsilon^2 x\right)\left[1 - \cos\left(\omega_{pe,x} t\right)\right]\hat{\boldsymbol{x}}, \tag{8}$$

where $\omega_{pe,x} \equiv 1 + \epsilon x/2$ is the normalized plasma frequency based on the x dependent density, n, and $\tilde{f}_n$ is an oscillatory term described in the supplementary materials. It is evident that the electric field of this solution oscillates about

$$\boldsymbol{E} = -\left(\epsilon - \epsilon^2 x\right)\hat{\boldsymbol{x}}. \tag{9}$$

The space dependent frequency, $\omega_{pe,x}$, gives rise to increasingly shorter scale x variations of the electric field. These variations along x lead to phase mixing in space and then Landau damping. Our model does not show this damping because the damping is exponentially suppressed until $k\lambda_D \lesssim 1$ which occurs at $t \sim \epsilon^{-1}$ where the assumptions break down. Eventually Landau damping eliminates the oscillations, and thus the electric field should naturally settle to Eq. (9). If we take Eq. (9) as the initial condition for the electric field, we arrive at an equilibrium solution to Eqs. (4–6) where $\boldsymbol{E}$ and f do not change with time.

Temperature gradient. We now consider a second case, with a temperature gradient only ($\epsilon = 0$, $\delta \neq 0$). If we again start with the initial conditions $f = f_0$, and no initial electric or magnetic fields, to second order in δ, the solution to Eqs. (4–6) is the following:

$$f = f_{\nabla T} + \tilde{f}_T(t), \tag{10}$$

$$\boldsymbol{E} = -\delta\left[1 - \cos(t)\right]\hat{\boldsymbol{y}}, \tag{11}$$

where

$$f_{\nabla T} \equiv f_0 + \frac{1}{2}\delta t v_y \left(5 - v^2\right) f_M - \frac{1}{4}\delta^2 t y v_y \left(25 - 12v^2 + v^4\right) f_M + \delta^2 t^2 \left[\frac{1}{8} v_y^2 \left(39 - 14v^2 + v^4\right) - \frac{1}{4}\left(5 - v^2\right)\right] f_M, \quad (12)$$

and $\tilde{f_T}$ is an oscillatory term described in the supplementary materials. Once again the solution oscillates around a particular value for the electric field:

$$\boldsymbol{E} = -\delta \hat{\boldsymbol{y}}. \quad (13)$$

It is natural to start from Eq. (13) as an initial condition. This yields a simpler solution where the electric field is constant with time, but the distribution function continues to evolve with time as $f = f_{\nabla T}$.

Two important terms in Eq. (12) grow with t and eventually break the assumptions of the ordering. The second term on the RHS of Eq. (12) is associated with the heat flux, and matches the collisional solution shown in [13] once t reaches the collision time. However the assumptions will have already broken when $t \sim \delta^{-1}$. The fourth term on the RHS of Eq. (12), which grows as t^2 is associated with a temperature anisotropy, where the collisionless temperatures in each direction (corresponding to diagonal components of the pressure tensor) differ. This term breaks the assumptions earlier; when $t \sim \delta^{-1/2}$. However, the simulations will show that the predictions remain valid beyond this limit.

We define the pressure tensor (normalized to $m_e n_0 v_{T0}^2$) as:

$$nT_{ij} \equiv \int d^3 v v_i v_j f, \quad (14)$$

from which we find $T_{yy} = v_T^2 + 3/2\delta^2 t^2$ and $T_{xx} = T_{zz} = v_T^2 + 1/2\delta^2 t^2$, resulting in the following anisotropy:

$$A \equiv \frac{T_{yy}}{T_{xx}} - 1 = \delta^2 t^2. \quad (15)$$

The temperature gradient thus naturally leads to a temperature anisotropy. Hot particles with more momentum directed against the gradient arrive faster than other angles. This anisotropy will give rise to kinetic instabilities such as the Weibel instability [12] seen in [9] or instabilities that inhibit the heat flux [13, 14].

Eq. (15) is consistent with the anisotropy and the subsequent development of the Weibel instability obtained in the PIC simulations reported in [9] — see Fig. 1. The onset time of the Weibel instability τ_W is roughly estimated from the magnetic energy spectra when the Weibel field begins to grow exponentially. Fig. 1(a) shows the spectra for the case where $L_T/d_e = 400$ ($\delta^{-1} = 2000$), with the onset of Weibel indicated by a dashed line. Although the Biermann field is energetically dominant for

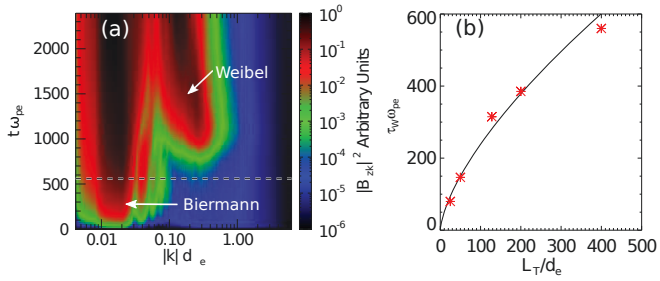

FIG. 1. (a) Magnetic energy spectra of B_z (with respect to $|k| = \sqrt{k_x^2 + k_y^2}$) vs. time from the simulation with system size $L_T/d_e = 400$ ($L_T/\lambda_D = 2000$) reported in Ref. [9]. The time when the Weibel instability begins to grow exponentially is identified with a dashed line. This estimate of the onset time τ_W is plotted vs. system size (b) along with the predicted curve where Eq. (16) is satisfied indicating where the Weibel growth rate exceeds that of the anisotropy predicted in Eq. (15).

smaller system sizes, the higher k Weibel instability is present (i.e. an onset time can be measured) for all simulations. The onset time, τ_W, should occur when the Weibel growth rate, which is a function of anisotropy, and thus of time, exceeds the predicted rate of anisotropy growth from Eq. (15):

$$\gamma_W(A(\delta t)) > 1/A\partial A/\partial t = 2/t. \quad (16)$$

Fig. 1(b) shows that this prediction matches the estimated onset over a range of system sizes remarkably well, where $\gamma_W(A)$ is the growth rate of the Weibel instability, given by [12], which we solve numerically. γ_W is calculated at the location of fastest growth ($x/L_T = 0.9125, y/L_T = 0$), which is independent of system size using the local values; $v_T = 0.036c$, $n = 0.12n_0$, and the anisotropy calculated from Eq. (15) using $L_{T,local} = 0.0625 L_T$ and v_T. Note that this anisotropy is slightly increased by a factor of 5/4 to take into account second order variations in temperature [17]; this is addressed in [11].

It is surprising that the agreement is so good since these simulations are in highly nonlinear regimes; the assumption that $\tau_W \ll \delta^{-1}$ is only satisfied for sufficiently large L_T/d_e. For the largest $L_T/d_e = 400$ case ($\tau_W \omega_{pe,local} \approx 0.8\delta_{local}^{-1}$), nonlinear effects were clearly present. The thermal velocity, which we assume to be constant with time except for the small modification $\sim \delta^2 t^2$, grew as $v_T \sim t$. The measured anisotropy grew at close to $A \sim t^4$, which is still consistent with $A = \delta^2 t^2$, given that δ is now a function of time. We expect the onset time to continue to follow this trend for even larger L_T, where our assumption $\tau_W \omega_{pe,local} \ll \delta_{local}^{-1}$ is valid.

Biermann battery. Both of these simplified cases oscillate about the equilibrium electric fields, Eq. (9) and Eq. (13), and Landau damping eventually eliminates

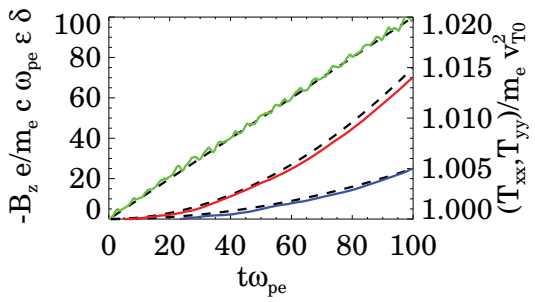

FIG. 2. Evolution of the averaged B_z due to the perpendicular density and temperature gradients (green), and anisotropic temperatures T_{xx} (blue) and T_{yy} (red), vs. time along with the predicted curves at $y = 0$ from Eq. (19) and Eq. (14) (black dashed lines).

these oscillations. Note that these equilibrium fields begin to balance the associated pressure gradients at a timescale of the electron plasma frequency $\sim \epsilon^0$; much smaller than the time scale of the Biermann battery (on the order of the electron transit time $L_T/v_{T0} \sim \epsilon^{-1}$). To simplify the solution and avoid the oscillations, we start with a similar electric field for the initial conditions for the complete case ($\epsilon \neq 0$, $\delta \neq 0$):

$$\boldsymbol{E} = -\left(\epsilon - \epsilon^2 x + \epsilon\delta y\right)\hat{\boldsymbol{x}} - \delta\hat{\boldsymbol{y}}. \tag{17}$$

With this assumption, and starting with f_0, the solution to Eqs. (4–6) is:

$$f = f_{\nabla T} + \frac{1}{2}\epsilon\delta t x v_y\left(5 - v^2\right) f_M + \frac{1}{2}\epsilon\delta t^2 v_x v_y f_M, \tag{18}$$

with the magnetic field:

$$\boldsymbol{B} = -\epsilon\delta t\hat{\boldsymbol{z}}, \tag{19}$$

where the electric field does not change with time.

We thus see a fully kinetic Biermann battery: the magnetic field grows linearly in time, and is proportional to both the density and temperature gradients, as in the fluid case.

Numerical comparison. Our analytic model has been tested via particle-in-cell (PIC) simulations using the OSIRIS framework [18, 19]. The simulations are done setting $\epsilon = \delta = 0.001$, and a normalized thermal velocity $v_{T0}/c = 0.05$, which is small such that relativistic effects do not play a role, but large compared to ϵ. A more detailed explanation of the simulation parameters and setup is outlined in the supplementary materials

To test these solutions we look at both simulations with $\delta = 0$ or $\epsilon = 0$, and with both gradients. Good agreement between the predicted and simulated electric fields for single gradients is shown in the supplementary materials. In Fig. 2 the average magnetic field from the simulation with both gradients grows linearly in time, confirming the prediction in Eq. (19). The growth of the temperatures in the x and y directions shown in Fig. 2 matches quite well with the predictions from Eq. (14). Note that our solution is rigorously only valid for $t \ll \delta^{-1/2} = 50$, but this breaking would occur at many more ω_{pe}^{-1} for realistically small values of δ that are not feasible to simulate. The plotted simulation fields are calculated by averaging the results between $-49 < x < 49$, and $-49 < y < 49$.

Conclusions. In this Letter, we have presented analytical solutions of the Vlasov-Maxwell system of equations for collisionless systems with background density and temperature gradients. The kinetic equivalent of the Biermann battery — a linear in time magnetic field growth — has been obtained for the first time. Another noteworthy result is the generation of temperature anisotropy in all cases where a background temperature gradient is present. This implies that pressure anisotropy driven instabilities, such as electron Weibel, should be expected in such systems. These may have a profound impact on their evolution, from effectively determining the magnetic field growth, to constraining the heat flux.

Although this Letter does not consider anisotropies generated by an initial velocity shear [20–22] (as opposed to a temperature gradient), in certain cases this effect may compete with our predicted anisotropy.

Formally the initial non-equilibrium state is taken to be generated such that the time scale for the change in temperature and density is fast compared to the electron plasma frequency. On the other hand, the time scale for the generation of these gradients, which happens for example in laser or shock interactions, is often similar or longer than the period of plasma oscillations. However, the interaction with the more slowly generated gradients would only lead to plasma oscillations comparable to those which we have shown are excited by our initial conditions. In effect, we model the time scale that is slow compared to the gradient generation, but fast compared to the electron transit time L_T/v_{T0}. Although as seen above in simulations, even when the gradients grow on the same order as L_T/v_{T0} ($\delta \propto t$) the evolution of anisotropy continues to follow Eq. (15), with $A \sim \delta\,(t)^2\, t^2$.

It should be noted that for simplicity, there are a few limitations to the generality of this work. The pressure and density gradients are assumed to be perpendicular, and the gradients are entirely linear, not including second order variation. The more general case is found in [11].

However, this solution remains quite general. An anisotropic Maxwellian distribution ($v_{Ti0} \neq v_{Tj0}$, where v_{Ti0} is the thermal velocity in the i direction) can be modeled by the same equations; this better approximates the initial conditions generated by laser-plasma interactions. In the anisotropic case, $\boldsymbol{x}$, $\boldsymbol{v}$, and $\boldsymbol{E}$ are normalized using the v_{Ti0} in the corresponding direction, and Eq. (19) has an additional factor of v_{Tx0}/v_{Ty0}.

This means that the Biermann field is caused solely by the thermal spread directed along the density gradient (v_{Tx0}). Furthermore, the anisotropy starting from an initially anisotropic bi-Maxwellian system with $A = A_0$ evolves as $A = A_0 + \delta^2 t^2 (1 + A_0)(1 - A_0/2)$. This expression implies that the anisotropy is limited to grow larger for $A_0 < 2$. The anisotropy A, however, may surpass this limit because A_0 is assumed to be initially based on a bi-Maxwellian and constant in space and time.

Moreover, the kinetic result of anisotropy generation is relevant even for magnetized cases, as long as the temperature gradient is parallel to the magnetic field. Our solution for the case with $\epsilon = 0$ is valid for a uniform parallel magnetic field of arbitrary magnitude. For significantly large fields, instabilities driven by the anisotropy in a magnetized plasma, such as the firehose instability [23], would dominate over the Weibel instability.

Anisotropy driven instabilities can help explain weak heat fluxes in cooling flows. Another kinetic instability that can lead to suppression in heat flux is driven solely by the heat flux [24] with a growth rate $\gamma_{HF} \approx 0.1\Omega_{ce}\epsilon_{HF}$, where Ω_{ce} is the electron cyclotron time and ϵ_{HF} is the coefficient proportional to the heat flux taken from [24]. The second term on the RHS in Eq. (12) corresponds to $\epsilon_{HF} = \sqrt{2}\delta t$. We can estimate the onset time $\tau_{HF} \approx 2.7(\delta\Omega_{ce})^{-1/2}$ of this instability by comparing the predicted heat flux growth $1/\epsilon_{HF}\partial\epsilon_{HF}/\partial t = 1/t$, to γ_{HF}.

Comparing the onset time of the heat flux instability to the Weibel $\tau_W \approx 1.6(\delta^3 v_T/c)^{-1/4}$ (in the limit $A \ll 1$, where $\gamma_W(A) = (8/27\pi)^{1/2} A^{3/2} v_T/c$ [25]), reveals the Weibel instability will appear first as long as β_e, the ratio of the electron plasma pressure to the magnetic pressure, is sufficiently large; $\beta_e \gtrsim L_T/d_e$. The Biermann battery alone often grows slow enough that β_e remains larger before the Weibel onsets; as long as $\delta \lesssim 4((v_T/c)L_n/L_T)^4$, using τ_W in Eq. (19) to find β_e. Either of these instabilities is likely to cause the heat flux to saturate long before reaching the collision time.

The purely kinetic temperature anisotropy generation from temperature gradients is thus relevant for a wide variety of settings; from astrophysical shocks and laser experiments with small collision rates where the Biermann battery can also exist, to flux tubes [26, 27] with temperature gradients found in the solar corona or at the Earth's magnetopause.

Acknowledgments. This work was supported by the European Research Council (ERC-2010-AdG Grant No. 267841, and ERC-2015-AdG Grant No. 695008). NFL was partially funded by NSF CAREER award no. 1654168.

[1] R. M. Kulsrud and S. W. Anderson, Astrophys. J. **396**, 606 (1992).
[2] R. M. Kulsrud and E. G. Zweibel, Rep. Prog. Phys. **71**, 046901 (2008).
[3] J. A. Stamper, K. Papadopoulos, R. N. Sudan, S. O. Dean, and E. A. McLean, Phys. Rev. Lett. **26**, 1012 (1971).
[4] C. K. Li, F. H. Seguin, J. A. Frenje, J. R. Rygg, R. D. Petrasso, R. P. J. Town, O. L. Landen, J. P. Knauer, and V. A. Smalyuk, Phys. Rev. Lett. **99**, 055001 (2007).
[5] G. Gregori, A. Ravasio, C. Murphy, K. Schaar, A. Baird, A. Bell, A. Benuzzi-Mounaix, R. Bingham, C. Constantin, R. Drake, M. Edwards, E. Everson, C. Gregory, Y. Kuramitsu, W. Lau, J. Mithen, C. Niemann, H.-S. Park, B. Remington, B. Reville, A. Robinson, D. Ryutov, Y. Sakawa, S. Yang, N. Woolsey, M. Koenig, and F. Miniati, Nature **481**, 480 (2012).
[6] L. Gao, P. M. Nilson, I. V. Igumenshchev, M. G. Haines, D. H. Froula, R. Betti, and D. D. Meyerhofer, Phys. Rev. Lett. **114**, 215003 (2015).
[7] L. Biermann, Z. Naturforsch. **5a**, 65 (1950).
[8] In systems with large magnetic fields such that the Larmor radius is small compared to the system size (not relevant in this work) fluid models with a non-scalar pressure tensor aligned with the field can be formulated.
[9] K. M. Schoeffler, N. F. Loureiro, R. A. Fonseca, and L. O. Silva, Phys. Rev. Lett. **112**, 175001 (2014).
[10] K. M. Schoeffler, N. F. Loureiro, R. A. Fonseca, and L. O. Silva, Phys. Plasmas **23**, 056304 (2016).
[11] K. M. Schoeffler and L. O. Silva, Plasma Phys. Contr. Fusion **60**, 014048 (2018).
[12] E. S. Weibel, Phys. Rev. **114**, 18 (1959).
[13] A. Levinson and D. Eichler, Astrophys. J. **387**, 212 (1992).
[14] S. P. Gary and H. Li, Astrophys. J. **529**, 1131 (2000).
[15] A. C. Fabian, Annu. Rev. Astron. Astrophys. **32**, 277 (1994).
[16] Our calculation assumes $v_{T0}^2/c^2 \sim \epsilon^0$, although as long as $\boldsymbol{B} \sim \epsilon^2$ (as we find in our solution), it is acceptable for $v_{T0}^2/c^2 \sim \epsilon^1$.
[17] A second derivative of the temperature, which is greater along $\hat{x}$, leads to a temperature anisotropy hotter along $\hat{x}$. ($A = t^2(\partial^2 T/\partial x^2 - \partial^2 T/\partial y^2)/T$).
[18] R. A. Fonseca, L. O. Silva, F. S. Tsung, V. K. Decyk, W. Lu, C. Ren, W. B. Mori, S. Deng, S. Lee, T. Katsouleas, and J. C. Adam, Lect. Notes Comput. Sci. **2331**, 342 (2002).
[19] R. A. Fonseca, S. F. Martins, L. O. Silva, J. W. Tonge, F. S. Tsung, and W. B. Mori, Plasma Phys. Contr. Fusion **50**, 124034 (2008).
[20] S. S. Cerri, F. Pegoraro, F. Califano, D. D. Sarto, and F. Jenko, Phys. Plasmas **21**, 112109 (2014).
[21] S. De Camillis, S. S. Cerri, F. Califano, and F. Pegoraro, **58** (2015).
[22] D. Del Sarto, F. Pegoraro, and F. Califano, **93** (2016).
[23] E. N. Parker, Phys. Rev. **109**, 1874 (1958).
[24] G. T. Roberg-Clark, J. F. Drake, C. S. Reynolds, and M. Swisdak, Astrophys. J. Lett. **830**, L9 (2016).
[25] R. C. Davidson, D. A. Hammer, I. Haber, and C. E. Wagner, Phys. Fluids **15**, 317 (1972).

[26] E. N. Parker, *Cosmical magnetic fields: Their origin and their activity* (Oxford, Clarendon Press; New York, Oxford University Press, 1979) p. 858.
[27] C. T. Russell, E. R. Priest, and L. C. Lee, *Physics of magnetic flux ropes* (American Geophysical Union Washington, D.C, 1990) pp. xvi, 685.